

Molecular Mechanism of Transcription Inhibition by Peptide Antibiotic Microcin J25

Karen Adelman,^{1,2,*} Julia Yuzenkova,³ Arthur La Porta,² Nikolay Zenkin,³ Jookyung Lee,⁴ John T. Lis,¹ Sergei Borukhov,⁴ Michelle D. Wang,² and Konstantin Severinov^{3,*}

¹Department of Molecular Biology and Genetics

²Department of Physics

Laboratory of Atomic and Solid State Physics
Cornell University

Ithaca, New York 14853

³Department of Molecular Biology and Biochemistry
Waksman Institute

Piscataway, New Jersey 08854

⁴SUNY Health Sciences Center at Brooklyn
Brooklyn, New York 11203

Summary

21 amino acid peptide Microcin J25 (MccJ25) inhibits transcription by bacterial RNA polymerase (RNAP). MccJ25-resistance mutations cluster in the RNAP secondary channel through which incoming NTP substrates are thought to reach the catalytic center and the 3' end of the nascent RNA is likely to thread in backtracked transcription complexes. The secondary channel also accepts transcript cleavage factors GreA and GreB. Here, we demonstrate that MccJ25 inhibits GreA/GreB-dependent transcript cleavage, impedes formation of backtracked complexes, and can be crosslinked to the 3'-end of the nascent RNA in elongation complexes. These results place the MccJ25 binding site within the secondary channel. Moreover, single-molecule assays reveal that MccJ25 binding to a transcribing RNAP temporarily stops transcript elongation but has no effect on the elongation velocity between pauses. Kinetic analysis of single-molecule data allows us to put forward a model of transcription inhibition by MccJ25 that envisions the complete occlusion of the secondary channel by bound inhibitor.

Introduction

DNA-dependent RNA polymerase (RNAP), the central enzyme of bacterial gene expression, is a large, multi-subunit target for drug development (Darst, 2001). The catalytically competent core RNAP has subunit composition $\alpha_2\beta\beta'\omega$ and a total molecular weight near 400 kDa. Several antibiotics target RNAP and at least one, Rifampicin, has found wide use in clinical settings. Both recent advances in structural understanding of RNAP and the development of high-throughput screens promise to greatly enhance the development of additional drugs that target this important enzyme.

Drugs that have high specificity for RNAP have also proven to be extremely effective tools for probing transcription and regulation of this large machine. For exam-

ple, Rifampicin, a drug that specifically blocks RNAP initiation-to-elongation transition, has proven invaluable in probing the molecular mechanism of transcription initiation and promoter escape. Here we characterize a more recently identified antibacterial peptide Microcin J25 (MccJ25) that functions through inhibition of bacterial RNAP (Delgado et al., 2001; Yuzenkova et al., 2002). MccJ25 is a 21 amino acid, ribosomally synthesized peptide (Blond et al., 1999; Salomon and Farias, 1992) produced by strains of *Escherichia coli* harboring a plasmid-borne synthesis, maturation, and export system (Solbiati et al., 1999). Interestingly, the structure of MccJ25 exhibits a highly unusual threaded lasso fold (Bayro et al., 2003; Rosengren et al., 2003; Wilson et al., 2003). Understanding how this structure exerts its effect on RNAP will be important to both clinical applications and basic studies of transcription.

Mutations in RNAP that provide resistance to MccJ25 have provided clues to its mechanism of action. MccJ25-resistance mutations alter RNAP residues exposed on the inside of a 12–15 Å-wide secondary channel that branches off from the main active site channel (Yuzenkova et al., 2002). The secondary channel has been proposed to allow a path for nucleotide substrates to diffuse to the enzyme active site (Korzheva et al., 2000; Zhang et al., 1999). Furthermore, Korzheva et al. (2000) suggested that this secondary channel accepts the 3'-end-proximal portion of the nascent RNA in unproductive backtracked elongation complexes. Finally, three independent studies recently have shown that transcript cleavage factors GreA and GreB, which induce the endonucleolytic activity of the RNAP catalytic center and thus rescue backtracked complexes, bind within the secondary channel (Laptenko et al., 2003; Opalka et al., 2003; Sosunova et al., 2003).

In this work, we studied the consequences of MccJ25 addition on functional properties of RNAP in vitro using biochemical and single-molecule biophysical approaches. Our results support the idea that MccJ25 binds within the RNAP secondary channel and, when bound, completely prevents traffic through the channel. The results are in agreement with the conclusions of the accompanying paper, Mukhopadhyay et al., 2004. The implications of this novel form of transcription inhibition on the mechanisms of RNAP elongation are discussed.

Results

Biochemical Data Position MccJ25 in the RNAP Secondary Channel

We have previously shown that MccJ25 inhibits abortive initiation by *E. coli* RNAP and that this inhibition occurs even when MccJ25 is added after promoter complex formation (Yuzenkova et al., 2002), consistent with the idea that MccJ25 targets either a catalytic step of the nucleotide addition reaction or interferes with substrate entry. Figure 1A shows the effect of MccJ25 on processive pyrophosphorolysis, a reaction that is the opposite of phosphodiester bond formation and that consists

*Correspondence: severik@waksman.rutgers.edu (K.S.); ka42@cornell.edu (K.A.)

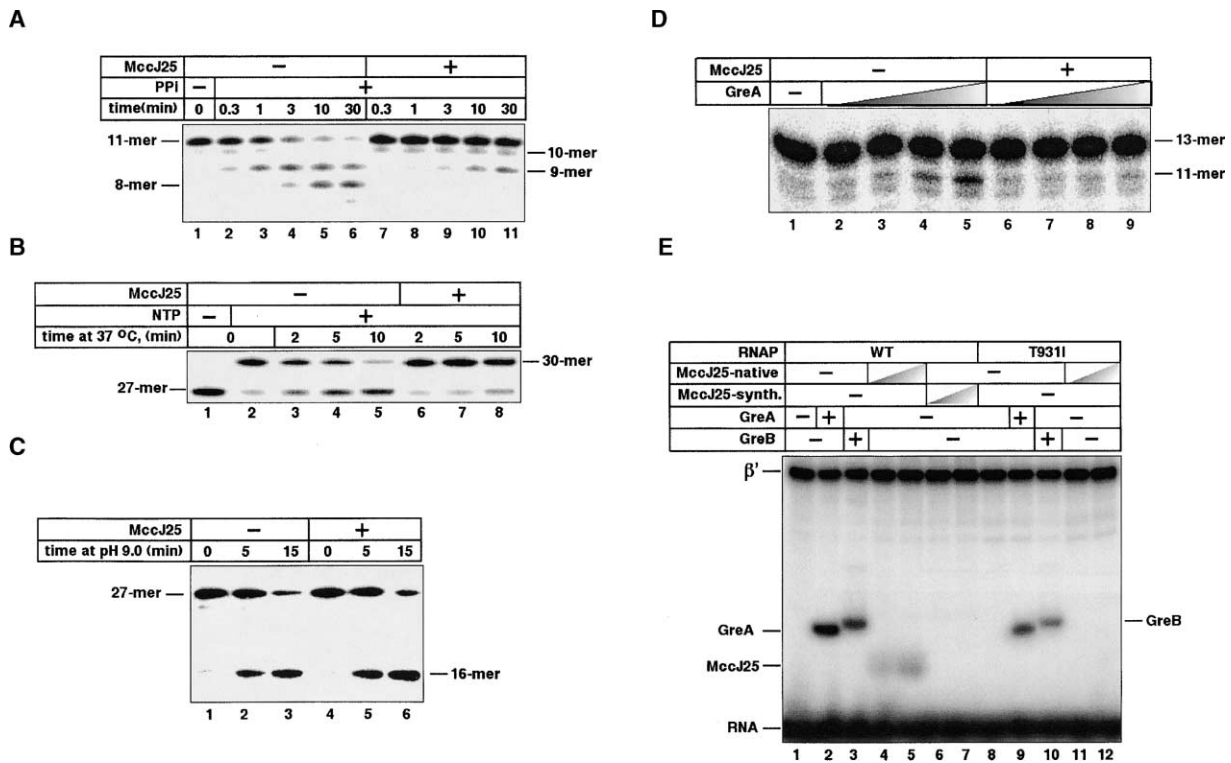


Figure 1. Biochemical Analysis of Transcription Inhibition by MccJ25

(A) MccJ25 inhibits processive pyrophosphorolysis. Stalled EC¹¹ were incubated in the presence of pyrophosphate with or without 50 μM MccJ25. At the times indicated, aliquots were removed and reactions terminated. Reaction products were analyzed by denaturing PAGE and revealed by PhosphorImager.

(B) MccJ25 inhibits backtracked complex formation. Stalled EC²⁷ were formed on a T7 A1 promoter template. The complexes were incubated at 37°C in the absence of NTPs for the times indicated with or without 25 μM MccJ25. The complexes were then supplied with CTP and incubated for an additional 2 min.

(C) MccJ25 has no effect on intrinsic endonucleolytic cleavage by RNAP. Backtracked EC²⁷ were obtained and transferred to a pH 9.0 buffer. EC²⁷ were incubated for the times indicated in the presence or absence of 25 μM MccJ25.

(D) MccJ25 decreases the rate of GreA-catalyzed endonucleolytic cleavage. Transcription complexes assembled on a minimal nucleic acid scaffold (Sidorenkov et al., 1998) were incubated in the presence of increasing concentrations of recombinant GreA protein, with or without MccJ25.

(E) MccJ25 contacts the 3' end of the nascent RNA. EC⁷ containing wild-type or mutant, MccJ25-resistant T931I RNAP, were formed on a *rrnB* P1 promoter template. The RNA contained a crosslinkable group at its 3'-end. EC⁷ were supplemented as indicated and crosslinks induced by UV-irradiation. Reaction products were separated by SDS-PAGE and revealed by PhosphorImager.

of attack by inorganic pyrophosphate on the 3-end of the nascent RNA, followed by NTP release and backward translocation of the elongation complex (EC). Stalled EC containing radioactively labeled 11 nt-long nascent RNA (EC¹¹) were prepared by nucleotide deprivation; EC¹¹ were washed to remove unincorporated NTPs and supplied with pyrophosphate in the presence or in the absence of MccJ25. In the absence of MccJ25, nascent RNA was progressively shortened and most of the initial transcript was replaced in 3 min by an 8 nt-long product (Figure 1A, lanes 1–6) (this product is released from the complex and is thus not a substrate to further pyrophosphorolysis). In the presence of MccJ25, pyrophosphorolysis was less efficient; even after a 30 min incubation in the presence of pyrophosphate most EC contained 11 nt-long RNA (Figure 1A, compare lanes 6 and 11). We conclude that MccJ25 inhibits both the forward reaction of phosphodiester bond synthesis and the reverse reaction of pyrophosphorolysis, a behavior expected of a drug that either affects RNAP catalytic

center or prevents the substrate and product traffic to/from the catalytic center.

Figure 1B shows the effect of MccJ25 on the formation of backtracked, arrested complexes. EC stalled at position 27 of a T7 A1 promoter-containing template (EC²⁷) were prepared and incubated in the absence of NTPs. During this incubation, EC²⁷ undergo backtracking and lose the ability to elongate the nascent RNA when NTPs are added. As can be seen from Figure 1B, ~95% of freshly prepared EC²⁷ were competent to resume transcription and elongate to position +30 upon addition of CTP (Figure 1B, lane 2; no further elongation occurred since template position 31 specifies a uridine, which is missing from the reaction), while the remaining 5% of the EC remained at position 27. The proportion of EC²⁷ capable of elongation decreased markedly after prolonged incubation in the absence of NTPs: after a 10 min incubation ~90% of EC²⁷ was arrested and unable to elongate the nascent transcript (Figure 1B, lane 5). When freshly prepared EC²⁷ was combined with 25 μM

MccJ25 prior to a 10 min incubation in the absence of NTPs, elongation-competent complexes persisted longer and 85% of EC²⁷ remained able to elongate the nascent transcript (Figure 1B, lane 8) (note that in this experiment, the concentration of CTP added during the chase step was high enough that elongation proceeded even in the presence of MccJ25). These results suggest that MccJ25 inhibits transcription arrest by preventing backtracking.

During backtracking, the portion of the nascent transcript that is proximal to the 3'-end is thought to be threaded into the RNAP secondary channel. The EC²⁷ complex formed at the T7 A1 promoter backtracks by 11 nucleotides, juxtaposing the catalytic center in the arrested state with the phosphodiester bond between RNA positions 16 and 17 (Komissarova and Kashlev, 1997). Backtracked EC²⁷ can be rescued by an endonucleolytic cleavage reaction catalyzed by the RNAP active site. The reaction is stimulated by mildly basic pH (Orlova et al., 1995) and generates two RNA fragments. The 3'-proximal 11 nt-long RNA fragment is released from the EC, while the 16 nt-long 5'-end-fragment remains bound by RNAP. The newly formed 3'-end is thus aligned with the active site and can be further elongated (Surratt et al., 1991). If MccJ25 binds within the secondary channel, one might predict that MccJ25 should not affect the endonucleolytic cleavage activity of RNAP in fully backtracked EC²⁷ complexes, because the 3'-portion of the nascent RNA would occupy the MccJ25 binding site. Indeed, as is shown in Figure 1B, pH 9.0-induced cleavage of the nascent RNA in arrested EC²⁷ proceeded at a similar rate in the absence or in the presence of MccJ25 (Figure 1B, compare the corresponding lanes 2 and 5, 68% and 55% of residual EC²⁷; and lanes 3 and 6, 13% and 15% residual EC²⁷, respectively).

The endonucleolytic activity of RNAP is enhanced by transcript cleavage factors GreA and GreB (Borukhov et al., 1992). Gre factors insert their long coiled-coil domain into the secondary channel, reaching into the catalytic center to help coordinate a Mg²⁺ ion necessary for the endonucleolytic cleavage reaction (Laptenko et al., 2003; Opalka et al., 2003; Sosunova et al., 2003). MccJ25 binding in the secondary channel might affect Gre factor-dependent cleavage by blocking access of Gre factors to the catalytic center. To evaluate this possibility, an artificial EC¹³ was assembled using a nucleic acid scaffold containing a 30 nt-long template-strand DNA oligonucleotide, fully complementary non-template DNA oligonucleotide, and a 13 nt-long RNA that was radiolabeled at the 5'-end (Sidorenkov et al., 1998). Addition of increasing amounts of recombinant GreA to these assembled EC¹³ resulted in the appearance of 11 nt-long cleavage products (Figure 1D, lanes 2–5). The cleavage reaction was dependent on both GreA and RNAP (data not shown), indicating that only RNA assembled in EC was cleaved and that the EC¹³ were backtracked by two nucleotides. Simultaneous addition of GreA and MccJ25 to preformed EC inhibited the cleavage of the 13 nt-long RNA (Figure 1D, compare, for example, lanes 5 and 9; 8 and <1% cleavage of initial EC¹³), indicating that MccJ25 interferes with Gre factor-dependent cleavage.

To test directly whether MccJ25 binds in the second-

ary channel, a crosslinking experiment was performed. EC⁷ were prepared on an *rnnB P1* promoter-containing template (Borukhov et al., 1993). The nascent RNA was radioactively labeled and contained photoreactive, crosslinkable 4-thiouridine, instead of uridine, at the 3' end. Upon UV irradiation of such EC⁷, extensive radioactive labeling of the β' subunit was observed (Figure 1E, lane 1). When the crosslinking experiment was repeated with the addition of Gre factors prior to irradiation (the reaction buffer contained no Mg²⁺ to prevent Gre-induced cleavage of the nascent transcript), the anticipated radioactive labeling of Gre factors was observed (Figure 1E, lanes 2 and 3). The crosslinked site in the Gre factors was previously mapped to a basic patch region in the coiled-coil domain of Gre (Koulich et al., 1997; Stebbins et al., 1995) that protrudes inside the secondary channel according to low-resolution models of RNAP-Gre complex (Laptenko et al., 2003; Opalka et al., 2003; Sosunova et al., 2003). Identical crosslinking experiments performed in the presence of native MccJ25 showed a weak but reproducible radioactive band of ~8 kDa; increasing concentrations of MccJ25 lead to increased crosslinking efficiencies (Figure 1E, compare lanes 4 and 5). We interpret this band as a crosslink between MccJ25 (2.5 kDa) and the 7 nt-long RNA (3 kDa). Importantly, no 8 kDa band was visible when synthetic, circular MccJ25, which is chemically identical to native peptide but is biologically inactive, was used in crosslinking experiments (Figure 1E, lanes 6 and 7). Moreover, the 8 kDa band was also absent when the crosslinking reactions contained native MccJ25 and EC formed by mutant RNAP harboring a T931I substitution in β' , that makes RNAP resistant to MccJ25 (Figure 1E, lanes 11 and 12) (Yuzenkova et al., 2002). These results thus demonstrate that the 3'-end of the nascent RNA in these active EC⁷ is close to, or in contact with, bound MccJ25. Protein-RNA crosslinking studies establish that the 3'-end of the nascent RNA is also close to the β' G loop and the F helix (Borukhov et al., 1991; Markovtsov et al., 1996; Epshtein et al., 2002), two structural elements that are part of the secondary channel (Figure 2). We therefore infer, by extension, that MccJ25 binds within the secondary channel.

Kinetics of Transcription Inhibition by MccJ25

Taken together, the biochemical data presented in Figure 1 strongly suggest that MccJ25 binds in the secondary channel and that amino acid substitutions in the secondary channel that lead to MccJ25-resistance define the MccJ25 binding site. If the secondary channel serves as a conduit for NTP substrates, and if MccJ25 binding partially occluded the channel, inhibition by MccJ25 might be overcome at saturating NTP concentrations. However, as can be seen from Figure 2, MccJ25 can be docked fully within the secondary channel with little or no steric clashes. As a result, the opening of the channel would become wholly occluded, raising the possibility that MccJ25 inhibits transcription elongation by completely preventing reactant traffic through the channel.

To evaluate MccJ25's ability to inhibit nucleotide traffic, we investigated the kinetics of the abortive synthesis of a CpApU trinucleotide by the RNAP from the T7 A1

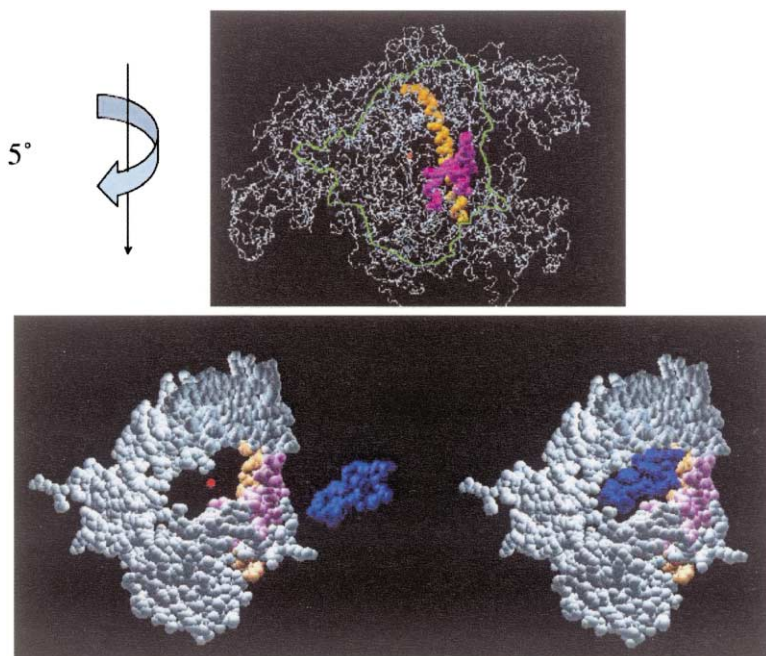


Figure 2. MccJ25 Binding Could Completely Block the Secondary Channel

(Top) Crystal structure of *Thermus aquaticus* RNAP at 3.3 Å resolution (Zhang et al., 1999). The bridge helix is shown in orange, G loop is shown in pink, and active site Mg^{2+} is depicted as a red sphere. The green contour encompasses RNAP elements that together form the secondary channel.

(Bottom left) The part of RNAP highlighted by the green contour at the top of the figure is shown in spacefill next to a spacefill model of the MccJ25 structure (Wilson et al., 2003) shown in blue.

(Bottom right) The MccJ25 structure docked within the RNAP secondary channel. A similar model could be built using the *T. thermophilus* RNAP holoenzyme structure (Vassylyev et al., 2002).

promoter. The reactions contained saturating amounts of CpA dinucleotide primer and increasing concentrations of the UTP substrate (see Supplemental Figure S1 at <http://www.molecule.org/cgi/content/full/14/6/753/DC1>). In the absence of MccJ25, the reaction was characterized by an apparent K_m value of $1.5 \pm 0.3 \mu M$, whereas in the presence of MccJ25 at $10 \mu M$, the apparent K_m increased more than 7-fold (Supplemental Figure S1). In addition, the maximum amount of CpApU synthesized decreased modestly (1.5-fold) in the presence of $10 \mu M$ MccJ25 (Supplemental Figure S1). Thus, although the primary effect of MccJ25 binding is an increased K_m for NTPs, MccJ25 exhibited a mixed mode of inhibition of the abortive initiation reaction at this promoter.

To gain further insight into the nature of MccJ25 inhibition, we investigated the effects of MccJ25 on transcription elongation under conditions that approximate physiological NTP concentrations. These experiments probe the interaction between MccJ25 and RNAP when the substrate is in excess of the average K_m for NTPs and the reaction generally proceeds at V_{max} . Radiolabeled EC²⁰ formed at the T7 A1 promoter (Figure 3, lane labeled EC²⁰) were washed, equilibrated to room temperature, and split into two equal reactions. The first reaction was restarted by addition of NTPs at 1 mM final concentration (Figure 3, -MccJ25, lanes 1–8) while the second reaction contained 1 mM NTPs plus $7.6 \mu M$ MccJ25 (+MccJ25, lanes 1'–8'). Aliquots of each reaction were taken and the reaction quenched at various time points to allow for investigation of the rate and efficiency of transcription as well as detection of transcriptional pauses. These data demonstrate three aspects of MccJ25 activity on EC: (1) MccJ25 significantly inhibits the overall rate of transcription elongation; (2) inhibition by MccJ25 occurs even in the presence of saturating NTP concentrations; and (3) the presence of MccJ25 enhances the appearance of transcriptional pauses. However, this assay does not allow us to determine

whether MccJ25 is causing additional pausing/stopping events, or is simply binding to RNAPs that are already paused at given locations and thereby enhancing the observed pause duration.

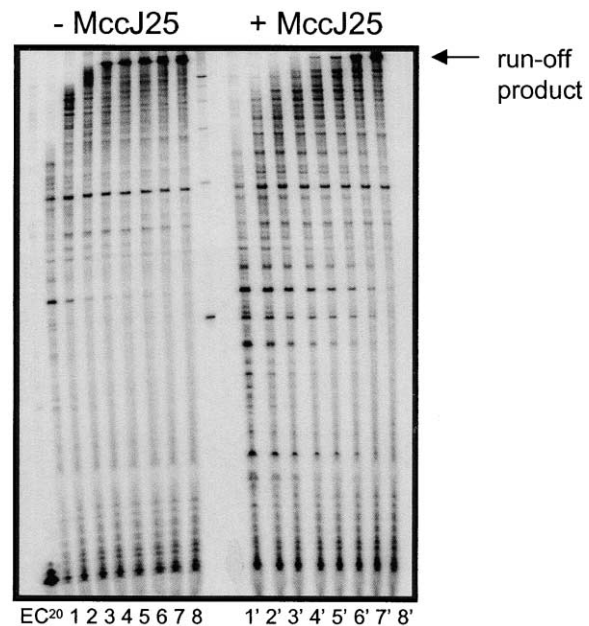


Figure 3. MccJ25 Inhibits Transcription Elongation at Saturating NTP Concentrations

Radiolabeled EC²⁰ were split into two reactions: one that was restarted by addition of 1 mM NTPs (-MccJ25, lanes 1–8) and the other with 1 mM NTPs and MccJ25 at a final concentration of $7.6 \mu M$ (+MccJ25, lanes 1'–8'). Aliquots were removed and the reaction stopped: 10, 20, 30, 40, 50, 60, 90, and 180 s after addition of NTPs. RNA products were separated by denaturing PAGE and visualized using a PhosphorImager. The position of the full-length, 900 nt product is shown at right.

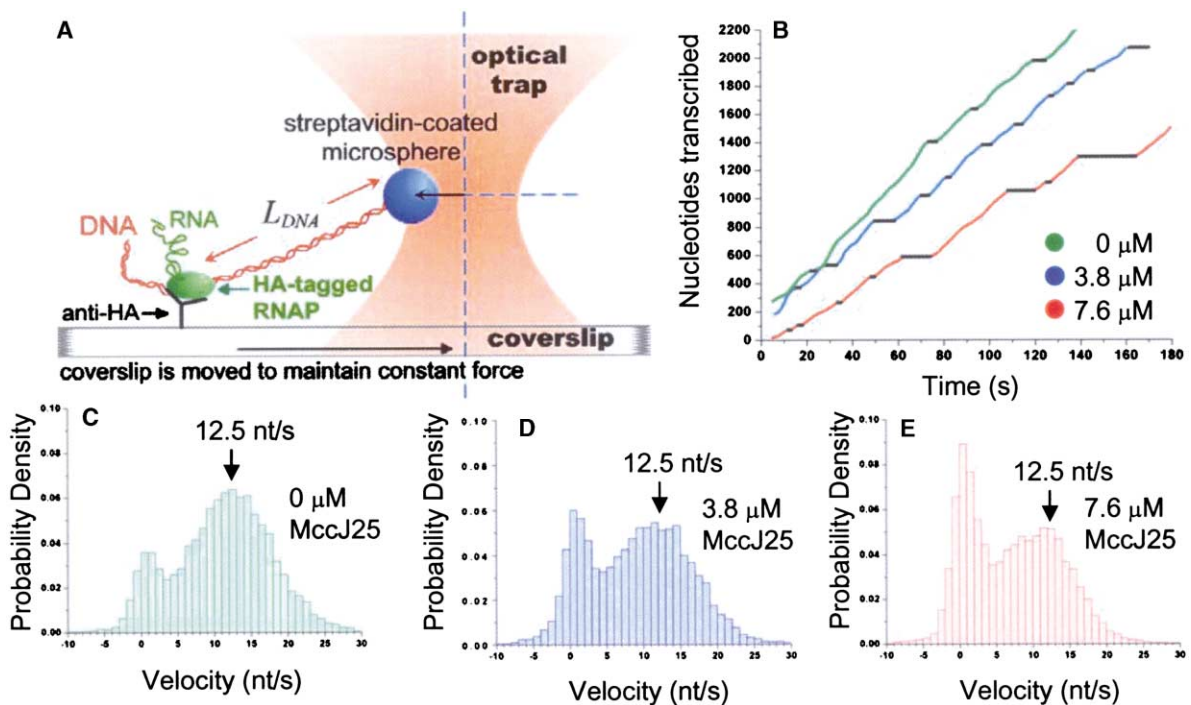


Figure 4. MccJ25 Increases RNAP Pausing without Altering Active Elongation Velocity

(A) Experimental setup for single molecule analyses of transcription elongation. Stalled EC²⁰ were prepared using a recombinant RNAP bearing the HA-epitope tag on an α -subunit. EC²⁰ were injected into a flow cell coated with antibody against the HA-epitope and a streptavidin-coated microsphere bound to a single biotin moiety at the downstream end of the template DNA (4.1 kb, containing the *rpoB* gene). Transcription was re-started by addition of NTPs at 1 mM in the presence or absence of MccJ25 at the concentrations noted. Elongation by the RNAP lead to a decrease in length of the DNA tether (L_{DNA}) that was detected in real-time by monitoring the position of the piezo stage and the displacement of the microsphere from the trap center as described in Adelman et al. (2002).

(B) Representative elongation profiles of transcription by individual RNAP molecules, plotted as nucleotides versus time (after applying our filtering procedure). The concentration of MccJ25 present is shown at right. Positions and durations of pauses detected are shown by black lines.

(C–E) Normalized probability distributions representing the fraction of time each RNAP population spends elongating at a given velocity: (C) in the absence of MccJ25; (D) at 3.8 μ M MccJ25; (E) at 7.6 μ M MccJ25. The distributions can each be fit by two Gaussian functions, with one component that represents active elongation velocities centered near 12.5 nt/s (shown by arrow), and one representing the inactive state, centered near 0 nt/s.

Analyzing the Effects of MccJ25 on Elongation by Single RNAP Molecules

The bulk assays presented above are limited by the complexity of the abortive initiation process (which makes it difficult to derive mechanistic insights from kinetic data) and do not allow one to distinguish between effects of MccJ25 on elongation rate, pause frequency, and pause duration. To probe these parameters, we undertook an analysis of elongation by single RNAP molecules in the presence of MccJ25 using optical trapping. This technique permits detection of elongation by individual RNAP in real-time, revealing the details of RNAP motion and the kinetic constants that define its transitions between active and inactive states. The experimental setup used is depicted in Figure 4A. A stalled EC²⁰ was specifically immobilized on the surface of a glass flow cell and re-started by addition of NTPs. RNAP movement was monitored throughout transcription elongation by measuring the decrease in length of the downstream DNA (L_{DNA}), as described previously (Adelman et al., 2002; Wang et al., 1997, 1998).

Elongation properties of 30 individual RNAP molecules observed in the absence of MccJ25 were compared to similar populations of RNAP in the presence

of either 7.6 μ M MccJ25 (as in Figure 3) or 3.8 μ M MccJ25. The overall elongation rates obtained for each population of RNAP molecules (total distance/total time) were as follows: 10.8 nt/s in the absence of MccJ25, 8.6 nt/s at 3.8 μ M MccJ25, and 7.0 nt/s at 7.6 μ M MccJ25. The decrease in overall transcription rates observed in the presence of MccJ25 demonstrates an effect on transcription elongation under single molecule conditions that is consistent with those observed in our bulk elongation assay. Figure 4B shows representative examples of elongation by individual RNAPs in the absence of MccJ25 (green line) and presence of MccJ25 at 3.8 μ M (blue line) or 7.6 μ M (red line). Elongation profiles are plotted as nucleotides transcribed versus time, with positions at which the RNAP halts transcription denoted by black lines (Experimental Procedures, Adelman et al., 2002). While the presence of MccJ25 noticeably increases the appearance of pausing/stopping events, the active elongation velocity (represented by the slope of the line between pauses) does not appear to be altered by MccJ25. These results suggest that MccJ25 binding induces the RNAP to stop rather than merely to slow transcription.

To evaluate whether this is generally true of the RNAP

observed in the presence of MccJ25, we plotted the combined distributions of instantaneous velocities of elongation for RNAP observed under each condition (Figures 4C–4E). The instantaneous velocity of elongation of individual RNAP was calculated from the traces of nucleotides transcribed versus time using an algorithm that effectively applies a Gaussian low-pass frequency filter to the position versus time data (Adelman et al., 2002). The resulting normalized probability distributions reflect the fraction of time that each RNAP population elongates at a given velocity. In agreement with our previous results, the velocity distribution obtained in the absence of MccJ25 is characterized by two components: one that represents the active elongation velocity between pauses, centered around 12.5 nt/s (shown by arrow), and another that represents the paused or inactive state, centered near 0 nt/s (Figure 4C; Adelman et al., 2002). Analysis of the velocity distributions obtained in the presence of MccJ25 reveals that the distribution of active elongation velocity remains centered near 12.5 nt/s (Figures 4D and 4E; Supplemental Figure S2), with the presence of MccJ25 eliciting no evident shift of elongation velocity toward slower levels. Instead, MccJ25 dramatically enhances the fraction of time the RNAP spends in an inactive state, as demonstrated by the marked increase in area under the peak at 0 nt/s. Neither the center nor the width of this distribution were altered by the presence of MccJ25, indicating that the velocity of a MccJ25-bound complex is indistinguishable from the paused state (Supplemental Data). These results argue against MccJ25 serving to only partially obstruct the secondary channel, as that would allow some substrate entry and thus some evidence of slow elongation to be observed. Moreover, because our filtering algorithm averages position using a Gaussian envelope with a standard deviation of 1 s, if MccJ25 binding and dissociation events were rapid (on a timescale of <1 – 2 s), they would be averaged together with RNAP movement to yield slow apparent elongation velocities. Thus, the complete block to transcription elongation observed in the presence of MccJ25 is consistent with a long-lived association of MccJ25 within the RNAP secondary channel (compared to our averaging time) that wholly occludes substrate entry.

Probing the Nature of MccJ25 Binding Events

The decrease in fraction of time the RNAP spends actively elongating in the presence of MccJ25 reflects the time that MccJ25 at that concentration is diverting the RNAP away from the productive state. To evaluate more precisely the effects of MccJ25 on this balance between active versus inactive states, we have employed a pause detection algorithm to determine the relative location and duration of pausing/stopping events by individual RNAPs (stopping events shown as black lines, Figure 4B, Adelman, et al., 2002). Whereas, in the absence of MccJ25, the RNAP population is actively elongating 77.1% of total time, this percentage decreases to 65.2% at 3.8 μ M MccJ25 and 54.9% at 7.6 μ M MccJ25, demonstrating that MccJ25 significantly reduces the time that the RNAP population is engaged in productive elongation (Supplemental Data). Assuming that the percent

decrease in time each RNAP population spends actively elongating at each MccJ25 concentration represents the time that otherwise active RNAP are bound and inhibited by MccJ25, we can derive an apparent K_i for the MccJ25•RNAP interaction under these conditions. Performing this calculation on both data sets obtained in the presence of MccJ25 (Supplemental Data) yields an average $K_i = 20 \mu$ M. We note that we cannot experimentally distinguish between MccJ25-bound and MccJ25-unbound states of a stopped RNAP, so that this value solely reflects the fraction of time that MccJ25 serves to prevent active elongation and does not explicitly measure the time that MccJ25 is bound to the RNAP.

By directly observing elongation and pausing by RNAP molecules in real-time, we are able to measure the microscopic rate constants for RNAP exiting and re-entering the productive elongation pathway. If MccJ25 binding to an actively elongating RNAP halts transcription, this would be detected in our assay as an increase in the frequency of stopping events observed in the presence of MccJ25. To evaluate this possibility, we analyzed the durations of time that each RNAP elongated between pausing/stopping events and compared the distributions obtained from each RNAP population (Figure 5A). In good agreement with previous data acquired in the absence of MccJ25, a fit of this distribution to a single exponential decay yields a half-life of active elongation between pauses of 12.1 s (Adelman et al., 2002). It has been previously demonstrated that the short pauses observed on this sequence (containing the *rpoB* gene from *E. coli*) are uncorrelated events that are randomly distributed over the template (within our 1 s time resolution; Adelman et al., 2002; Neuman et al., 2003). The distributions of times between pauses obtained in the presence of MccJ25 are also fit by exponential decay, suggesting that the MccJ25-induced stopping events are also likely to be randomly distributed. However, in the presence of MccJ25, the frequency of stopping events increases sharply (Figure 5A); at 7.6 μ M MccJ25 the RNAP population stops approximately twice as often as in the absence of MccJ25. Importantly, the observed half-life of active elongation shows a clear dependence on MccJ25 concentration, indicating that the rate being measured reflects an intermolecular interaction between MccJ25 and the RNAP.

If we attribute the increase in stopping events observed in the presence of MccJ25 directly to MccJ25 binding, the data presented in Figure 5A can be used to determine the rate of MccJ25 binding at each concentration (i.e., the rate of RNAP-stopping measured in the presence of MccJ25 = the rate of pausing observed in the absence of MccJ25 + the rate constant for MccJ25 binding at the given MccJ25 concentration). Determination of these MccJ25 binding rates at both concentrations allows us to calculate an apparent k_{on} for the MccJ25•RNAP interaction of $\sim 8 \times 10^3 \text{ M}^{-1}\text{s}^{-1}$ (Supplemental Data). This rate is extremely slow (compared to diffusion, which is 10^8 – $10^9 \text{ M}^{-1}\text{s}^{-1}$), which suggests that a productive MccJ25•RNAP interaction might transition through a slow intermediate, involve a conformational change or depend strongly upon molecular orientation during collision.

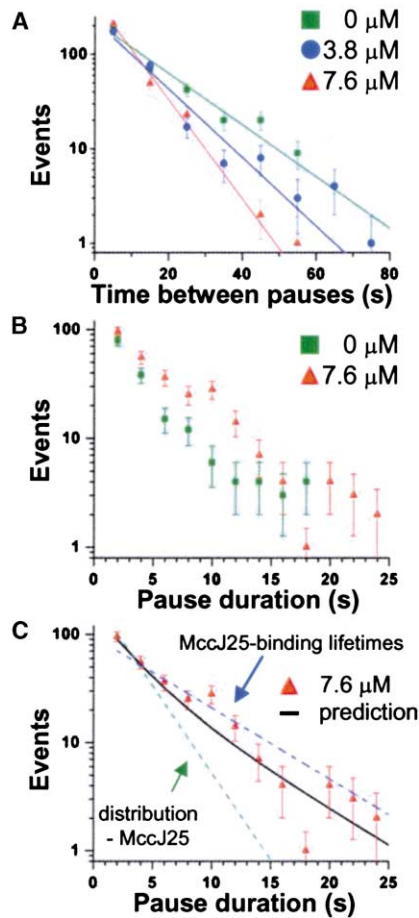


Figure 5. RNAP Stops Transcribing More Frequently in the Presence of MccJ25

(A) The number of RNAP-stopping events that occurred within a given time interval after the previous event is plotted versus time on a semilog graph (10 s bins) for each RNAP population. Single exponential fits of the data give lifetimes of active elongation between stopping events, shown as lines (0 MccJ25, $t_{1/2} = 12.1$ s, rate = 0.057 s $^{-1}$, reduced $\chi^2 = 3.1$; 3.8 μ M MccJ25, $t_{1/2} = 8.3$ s, rate = 0.083 s $^{-1}$, reduced $\chi^2 = 4.4$; 7.6 μ M MccJ25, $t_{1/2} = 5.7$ s, rate = 0.121 s $^{-1}$, reduced $\chi^2 = 1.6$).

(B) The observed pause durations are shown for RNAP in the presence of 0 MccJ25 (green squares) and 7.6 μ M MccJ25 (red triangles) as number of events observed vs. time (2 s bins).

(C) The distribution of pause durations at 7.6 μ M MccJ25 (red triangles) plotted as number of events versus time (2 s bins), is shown with the fit to single exponential decay for pause durations observed in the absence of MccJ25 (dotted green line; $t_{1/2} = 1.9$ s), the calculated distribution of MccJ25 binding lifetimes (dotted blue line; $t_{1/2} = 4.4$ s) and the predicted, dual exponential, distribution of pause durations derived from our model (solid black line). Our predicted distribution better reflects the observed data (the fit yields a reduced $\chi^2 = 2.9$), than does the MccJ25-independent pause lifetime (reduced $\chi^2 = 12.6$) or the calculated MccJ25 binding half-life (reduced $\chi^2 = 6.0$).

Duration of Stopping Events Observed in the Presence of MccJ25 Indicates a Long-Lived MccJ25•RNAP Interaction

A value for the duration of MccJ25 binding events was calculated using the apparent K_i and k_{on} described above and the simple formula $K_i \times k_{on} = k_{off}$. From these values,

we derive an apparent $k_{off} = 0.16$ s $^{-1}$, yielding an apparent MccJ25 binding half-life, $t_{1/2} = 4.4$ s. This lifetime is significantly longer than that characteristic of pausing on this sequence in the absence of MccJ25 (Figure 5B, green squares, fit to single exponential decay yields $t_{1/2} = 1.9$ s). Therefore, to test whether our assumptions lead to a model that is internally consistent, we evaluated our calculated MccJ25 binding half-life using the pause durations observed in the presence of MccJ25 at 7.6 μ M (Figure 5B). In agreement with a relatively long lifetime for MccJ25 binding events, there is an increased probability of longer pauses/stops in transcription at 7.6 μ M MccJ25 (Figure 5B, red triangles).

In addition, we made use of our prior analysis of the frequency of stopping events in the presence of MccJ25 (Figure 5A) and the fact that the distribution of pause durations at 7.6 μ M MccJ25 should represent a combination of short, MccJ25-independent pauses ($t_{1/2} = 1.9$ s) and longer MccJ25-induced stopping events ($t_{1/2} = 4.4$ s). The results in Figure 5A show that, at 7.6 μ M MccJ25, the RNAP population stops about twice as often, indicating that approximately half of the stopping events are MccJ25 dependent. Thus, the observed pause distributions at 7.6 μ M MccJ25 would be predicted to correspond to a dual exponential distribution of pause durations comprised of the two component lifetimes with equal weighting. Figure 5C shows the experimental data (red triangles, same as Figure 5B), while the black line represents the distribution predicted by our calculations. For comparison, Figure 5C also shows the fit to a single exponential decay of the MccJ25-independent pauses (green line, $t_{1/2} = 1.9$ s, from the data shown in Figure 5B) as well as the single exponential distribution indicated by our MccJ25 binding half-life (blue line, $t_{1/2} = 4.4$ s). While the observed pause durations fall between these two lifetimes, neither individual distribution is a good fit to the experimental data. In contrast, the observed experimental data at 7.6 μ M MccJ25 (red triangles) exhibits good agreement with the distribution of pause durations predicted by our model (black line), indicating that our model is consistent with all data observed.

Discussion

Recent advances in single molecule optical trapping techniques have allowed for direct observation of transcription elongation by individual RNAP molecules, yielding fundamental insight into mechanisms of RNAP movement (Adelman et al., 2002; Forde et al., 2002; Neuman et al., 2003; Shaevitz et al., 2003; Schafer, et al., 1991; Wang et al., 1998; Yin et al., 1995). We have used these novel techniques to monitor elongation by *E. coli* RNAP at varying concentrations of the transcription inhibitor MccJ25, measuring both the instantaneous velocity of RNAP elongation and the occurrence of transcriptional pauses. Following the motion of individual RNAP in real-time permits dissection of the effects of MccJ25 on pause frequency or duration from effects on the velocity of transcription elongation and allows for determination of the dynamics of MccJ25-RNAP interactions. Analysis of the instantaneous velocity distribu-

tions obtained in the presence of MccJ25 reveals that MccJ25 significantly increases the percentage of time the RNAP spends inactive, but has no effect on the velocity of active transcription elongation. Moreover, the distribution of velocity centered near 0 nt/s is not altered by MccJ25, which argues against even low levels of slow elongation by MccJ25-bound complexes (compare Figures 4C–4E). In fact, the inhibition by MccJ25 observed in single molecule assays appears binary in nature: the RNAP appears to be either completely unaffected by MccJ25, or the RNAP is totally inactive. The simplest interpretation of these data is that, during the active elongation observed, MccJ25 is not bound to the RNAP, but that binding of a single MccJ25 molecule is sufficient to immediately stop transcription elongation. This all-or-nothing style of inhibition thus indicates a 1:1 stoichiometry for the MccJ25-RNAP interaction and suggests that MccJ25 binding could act to entirely block traffic of NTPs through the secondary channel.

Understanding the mechanism of MccJ25 inhibition also requires knowledge of the specific targets of MccJ25-activity (i.e., identifying if MccJ25 binds to particular RNAP conformations). To evaluate whether MccJ25 can bind to and inhibit an active RNAP, we determined the frequency of pausing/stopping events in the presence of MccJ25. Analysis of the distributions of time that each RNAP population actively elongated between consecutive pauses showed that there is a striking increase in the frequency of stopping events observed in the presence of MccJ25, which is enhanced at higher MccJ25 concentrations (Figure 5A; data not shown). This concentration dependence of stopping events demonstrates that the rate being measured reflects an intermolecular interaction between MccJ25 and an actively elongating RNAP. Thus, these results are inconsistent with a model that envisions tight MccJ25 binding to the RNAP throughout elongation. Moreover, our data indicate that active EC are unlikely to be the sole targets of MccJ25 binding. The biochemical evidence presented in Figure 1 demonstrates that MccJ25 can bind to stalled EC and inhibit processive pyrophosphorylation and backtracking of the RNAP. In addition, inspection of the bulk assays of transcription elongation (Figure 3) suggests that MccJ25 also enhances the longevity of existent pauses, potentially through binding to an RNAP that is inactive and preventing it from resuming transcription. However, since MccJ25 binding has been shown to inhibit backtracking beyond several nucleotides (Figure 1B), it is unlikely that the RNAP would undergo arrest and/or significant movement with respect to the template DNA during such extended pauses.

The complete inhibition of transcription elongation elicited by MccJ25 could be the result of obstruction of the NTP uptake channel or could be caused by inhibition of catalysis and/or translocation (a combination of these two mechanisms is also possible). Strictly speaking, our data do not allow us to distinguish between these possibilities, though we currently favor the first possibility. The results of crosslinking experiments clearly show that MccJ25 binds within the secondary channel and the results of molecular modeling suggest that MccJ25 can completely obstruct the channel without contacting RNAP catalytic site, which is located much deeper in

the channel. Moreover, MccJ25-resistance mutations occur midway through the channel and throughout the secondary channel circumference. Since no MccJ25-RNA crosslinks are detected in transcription complexes formed by MccJ25-resistant RNAP, MccJ25-resistant mutations must abolish MccJ25 binding and therefore define the MccJ25 binding site.

We determine an apparent K_i for MccJ25 of approximately 20 μM at saturating NTP concentrations, in agreement with the accompanying paper (Mukhopadhyay et al.) that reports a K_D for the MccJ25-RNAP interaction of about 2 μM and an α value of ~ 10 . A relatively low overall affinity of MccJ25 for the RNAP could confer an advantage to MccJ25-producing cells, which lack resistance to MccJ25 (i.e., their RNAP are MccJ25 sensitive) and rely on an export pump to minimize the intracellular concentrations of MccJ25. In this way, a moderately weak MccJ25•RNAP interaction would allow intracellular MccJ25 levels that remain below a certain threshold to be tolerable to the MccJ25-producing cells. The fact that MccJ25-producing bacteria fail to accumulate mutations that render their RNAP MccJ25-resistant may suggest that such mutations could prove deleterious in a natural environment.

A key result of these studies is the identification of the RNAP secondary channel as a viable target for inhibitors of RNAP activity. Our data support the idea that this channel serves as a conduit for substrate entry and demonstrate that an inhibitor that binds within the channel can effectively inhibit transcription, even at saturating NTP concentrations. One current limitation of MccJ25 as a potential antibiotic is that it is only effective against RNAPs from gram-negative bacteria. However, characterization of the MccJ25 binding site and the dynamics of inhibition should facilitate selection or design of MccJ25 variants that can occlude the wider channels of Gram-positive bacteria and eukaryotes. Further structure-functional analysis of MccJ25 interactions within *E. coli* RNAP secondary channel should allow rational design of MccJ25-based RNAP inhibitors with broader specificity.

Experimental Procedures

Materials

MccJ25 was a gift of Dr. Raul Salomon, University of Tucuman, Argentina. MccJ25 was dissolved in water. The sample was pure as judged by the appearance of a single chromatographic peak during C18 reverse phase HPLC. The concentration of MccJ25 solution was determined by quantitative amino acid analysis (performed at the Protein Chemistry Laboratory of the University of Texas Medical Branch, Galveston, TX).

MccJ25-sensitive RNAP from *E. coli* AB259 cells and MccJ25-resistant RNAP carrying the T931 substitution in the β' subunit (from MccJ25-resistant *E. coli* SBG231 cells) were purified as described (Yuzenkova et al., 2002). MccJ25-sensitive GreA⁻/GreB⁻ RNAP was purified from AD8571 *E. coli* strain (Orlova et al., 1995). His-tagged GreA and GreB factors were purified as described (Koulich et al., 1997). RNAP bearing an HA-epitope tag on one α -subunit was purified as described in Adelman et al. (2002).

In Vitro Transcription

Pyrophosphorylation was performed using EC¹¹ prepared on a T7 A1 promoter-containing DNA template. EC¹¹ were prepared by supplying RNAP-promoter complexes formed in 10 μl of standard transcription buffer with 10 μM ApU initiating dinucleotide, 0.5 μM α -[³²P] ATP (3000 Ci/mmol), and 25 μM GTP. After 10 min incubation at 37°C, the reaction was supplemented with Ni²⁺-NTA-agarose

beads. After a 5 min incubation at room temperature, unincorporated substrates were washed away as described (Kashlev et al., 1996). One half of the reaction was supplemented with 50 μ M MccJ25, the other half was used as a control (no MccJ25 added). Sodium pyrophosphate was added to a final concentration of 100 μ M and aliquots were withdrawn at various times and combined with an equal volume of formamide-containing sample buffer. Products were resolved by Urea-PAGE and quantified using a PhosphorImager (Molecular Dynamics).

To obtain backtracked EC²⁷, the procedure of Komissarova and Kashlev (1997) was used. Aliquots of washed EC²⁷ were supplemented with 0 or 10 μ M MccJ25 and transferred to 37°C. After various incubation times, CTP was added to 25 μ M final concentration and incubation at 37°C was continued for 2 min. Reaction products were analyzed as above.

Elongation complexes on the artificial scaffold were assembled exactly as described in Sidorenkov et al., (1998). 0, 1, 5, 25, or 100 pmoles of GreA were added to 15 μ l reactions containing washed scaffolds. After 4 min at 37°C, reactions were stopped with formamide-containing loading buffer and products were analyzed as described above.

Bulk transcription assays were performed as described in Adelman et al. (2002), using a template containing the T7 A1 promoter upstream of the first 900 bp of the *rpoB* gene. The template was biotin labeled on the upstream end, to allow attachment to streptavidin coated microspheres. Radiolabeled EC²⁰ were washed to remove unincorporated nucleotides and transcription re-started at room temperature by the addition of NTPs to 1 mM with or without MccJ25 at 7.6 μ M. To allow for direct comparison with single molecule assays, these experiments were conducted with the RNAP bearing an HA-epitope tag on one α -subunit (Adelman et al., 2002).

Crosslinking Reactions

RNA-protein photo-crosslinking was performed using EC containing internally radiolabeled 7 nt long transcript carrying photoreactive 3'-terminal nucleotide, 4-thiouridine (7U^{*}-EC) as described (Borukhov et al., 2001). The identity and quantity of the resulting RNA products were verified by urea-23%-PAGE, and visualized by PhosphorImager. For each crosslinking reaction, 2.5 μ l aliquots (75–100 fmoles) of the 7U^{*}-EC were diluted into 10 μ l of incubation buffer (40 mM Tris-acetate [pH 7.9], 200 mM NaCl, and 10 mM EDTA) containing 0.2 mg/ml BSA and incubated for 5 min on ice in the wells of a standard 96-well microtiter plate alone or in the presence of purified GreA (1 μ g), GreB (0.2 μ g), natural or synthetic MccJ25 (1 and 4 μ g). The samples were UV irradiated and analyzed by 4%–20% gradient SDS-PAGE in MES-buffer system (Novex) as described in Borukhov et al. (2001).

Single-Molecule Transcription Assays

Single molecule transcription assays were performed as described in Adelman et al. (2002). Where indicated, MccJ25 at the given concentration was pre-mixed with NTPs before injection into the flow cell. Pause detection and velocity analysis was performed exactly as described in Adelman et al. (2002) except that pauses up to 200 s in duration were included in our present analyses. Additional information concerning data analysis and the determination of kinetic parameters is available in the Supplemental Text.

Acknowledgments

We thank Raul Salomon for providing us with purified MccJ25, Vitaly Epstein and Ekaterina Sosunova for advice, and Steve Koch, Richard Yeh, and Alla Shundrovskaya for construction of the optical trapping instrument. K.A. was supported by the National Research Service Award grant GM066661. This work was supported by NIH grants GM64503 (to K.S.), GM25232 (to J.T.L.), GM54098 (to S.B.), and GM59849A (to M.D.W.), by the Burroughs Wellcome Career Award (to K.S.) and Keck Foundation and Cornell's Nanobiotechnology Center (to M.D.W.).

Received: February 24, 2004

Revised: May 13, 2004

Accepted: May 21, 2004

Published: June 17, 2004

References

- Adelman, K., La Porta, A., Santangelo, T.J., Lis, J.T., Roberts, J.W., and Wang, M.D. (2002). Single molecule analysis of RNA polymerase elongation reveals uniform kinetic behavior. *Proc. Natl. Acad. Sci. USA* 99, 13538–13543.
- Bayro, M.J., Mukhopadhyay, J., Swapna, G.V., Huang, J.Y., Ma, L.C., Sineva, E., Dawson, P.E., Montelione, G.T., and Ebright, R.H. (2003). Structure of antibacterial peptide microcin J25: a 21-residue lariat protoknot. *J. Am. Chem. Soc.* 125, 12382–12383.
- Blond, A., Peduzzi, J., Goulard, C., Chiuchiolo, M.J., Barthelemy, M., Prigent, Y., Salomon, R.A., Farias, R.N., Moreno, F., and Rebuffat, S. (1999). The cyclic structure of microcin J25, a 21-residue peptide antibiotic from *Escherichia coli*. *Eur. J. Biochem.* 259, 747–755.
- Borukhov, S., Lee, J., and Goldfarb, A. (1991). Mapping of a contact for the RNA 3' terminus in the largest subunit of RNA polymerase. *J. Biol. Chem.* 266, 23932–23935.
- Borukhov, S., Polyakov, A., Nikiforov, V., and Goldfarb, A. (1992). GreA protein: a transcription elongation factor from *Escherichia coli*. *Proc. Natl. Acad. Sci. USA* 89, 8899–8902.
- Borukhov, S., Sagitov, V., Josaitis, C.A., Gourse, R.L., and Goldfarb, A. (1993). Two modes of transcription initiation in vitro at the *rmB* P1 promoter of *Escherichia coli*. *J. Biol. Chem.* 268, 23477–23482.
- Borukhov, S., Laptenko, O., and Lee, J. (2001). *Escherichia coli* transcript cleavage factors GreA and GreB: functions and mechanisms of action. *Methods Enzymol.* 342, 64–76.
- Darst, S.A. (2001). Bacterial RNA polymerase. *Curr. Opin. Struct. Biol.* 11, 155–162.
- Delgado, M.A., Rintoul, M.R., Farias, R.N., and Salomon, R.A. (2001). *Escherichia coli* RNA polymerase is the target of the cyclopeptide antibiotic microcin J25. *J. Bacteriol.* 183, 4543–4550.
- Epshtein, V., Mustaev, A., Markovtsov, V., Bereshchenko, O., Nikiforov, V., and Goldfarb, A. (2002). Swing-gate model of nucleotide entry into the RNA polymerase active center. *Mol. Cell* 10, 623–634.
- Forde, N.R., Izhaky, D., Woodcock, G.R., Wuite, G.J., and Bustamante, C. (2002). Using mechanical force to probe the mechanism of pausing and arrest during continuous elongation by *Escherichia coli* RNA polymerase. *Proc. Natl. Acad. Sci. USA* 99, 11682–11687.
- Kashlev, M., Nudler, E., Severinov, K., Borukhov, S., Komissarova, N., and Goldfarb, A. (1996). Histidine-tagged RNA polymerase of *Escherichia coli* and transcription in solid phase. *Methods Enzymol.* 274, 326–334.
- Komissarova, N., and Kashlev, M. (1997). Transcriptional arrest: *Escherichia coli* RNA polymerase translocates backward, leaving the 3' end of the RNA intact and extruded. *Proc. Natl. Acad. Sci. USA* 94, 1755–1760.
- Korzheva, N., Mustaev, A., Kozlov, M., Malhotra, A., Nikiforov, V., Goldfarb, A., and Darst, S.A. (2000). A structural model of transcription elongation. *Science* 289, 619–625.
- Koulich, D., Orlova, M., Malhotra, A., Sali, A., Darst, S.A., and Borukhov, S. (1997). Domain organization of *Escherichia coli* transcript cleavage factors GreA and GreB. *J. Biol. Chem.* 272, 7201–7210.
- Laptenko, O., Lee, J., Lomakin, I., and Borukhov, S. (2003). Transcript cleavage factors GreA and GreB act as transient catalytic components of RNA polymerase. *EMBO J.* 22, 6322–6334.
- Markovtsov, V., Mustaev, A., and Goldfarb, A. (1996). Protein-RNA interactions in the active center of transcription elongation complex. *Proc. Natl. Acad. Sci. USA* 93, 3221–3226.
- Neuman, K.C., Abbondanzieri, E.A., Landick, R., Gelles, J., and Block, S.M. (2003). Ubiquitous transcriptional pausing is independent of RNA polymerase backtracking. *Cell* 115, 437–447.
- Opalka, N., Chlenov, M., Chacon, P., Rice, W.J., Wriggers, W., and Darst, S.A. (2003). Structure and function of the transcription elongation factor GreB bound to bacterial RNA polymerase. *Cell* 114, 335–345.
- Orlova, M., Newlands, J., Das, A., Goldfarb, A., and Borukhov, S. (1995). Intrinsic transcript cleavage activity of RNA polymerase. *Proc. Natl. Acad. Sci. USA* 92, 4596–4600.
- Rosengren, K.J., Clark, R.J., Daly, N.L., Goransson, U., Jones, A.,

and Craik, D.J. (2003). Microcin J25 has a threaded sidechain-to-backbone ring structure and not a head-to-tail cyclized backbone. *J. Am. Chem. Soc.* *125*, 12464–12474.

Salomon, R.A., and Farias, R.N. (1992). Microcin 25, a novel antimicrobial peptide produced by *Escherichia coli*. *J. Bacteriol.* *174*, 7428–7435.

Schafer, D.A., Gelles, J., Sheetz, M.P., and Landick, R. (1991). Transcription by single molecules of RNA polymerase observed by light microscopy. *Nature* *352*, 444–448.

Shaevitz, J.W., Abbondanzieri, E.A., Landick, R., and Block, S.M. (2003). Backtracking by single RNA polymerase molecules observed at near-base-pair resolution. *Nature* *426*, 684–687.

Sidorenkov, I., Komissarova, N., and Kashlev, M. (1998). Crucial role of the RNA:DNA hybrid in the processivity of transcription. *Mol. Cell* *2*, 55–64.

Solbiati, J.O., Ciaccio, M., Farias, R.N., Gonzalez-Pastor, J.E., Moreno, F., and Salomon, R.A. (1999). Sequence analysis of the four plasmid genes required to produce the circular peptide antibiotic microcin J25. *J. Bacteriol.* *181*, 2659–2662.

Sosunova, E., Sosunov, V., Kozlov, M., Nikiforov, V., Goldfarb, A., and Mustaev, A. (2003). Donation of catalytic residues to RNA polymerase active center by transcription factor Gre. *Proc. Natl. Acad. Sci. USA* *100*, 15469–15474.

Stebbins, C.E., Borukhov, S., Orlova, M., Polyakov, A., Goldfarb, A., and Darst, S.A. (1995). Crystal structure of the GreA transcript cleavage factor from *Escherichia coli*. *Nature* *373*, 636–640.

Surratt, C.K., Milan, S.C., and Chamberlin, M.J. (1991). Spontaneous cleavage of RNA in ternary complexes of *Escherichia coli* RNA polymerase and its significance for the mechanism of transcription. *Proc. Natl. Acad. Sci. USA* *88*, 7983–7987.

Vassylyev, D.G., Sekine, S., Laptenko, O., Lee, J., Vassylyeva, M.N., Borukhov, S., and Yokoyama, S. (2002). Crystal structure of a bacterial RNA polymerase holoenzyme at 2.6 Å resolution. *Nature* *417*, 712–719.

Wang, M.D., Yin, H., Landick, R., Gelles, J., and Block, S.M. (1997). Stretching DNA with optical tweezers. *Biophys. J.* *72*, 1335–1346.

Wang, M.D., Schnitzer, M.J., Yin, H., Landick, R., Gelles, J., and Block, S.M. (1998). Force and velocity measured for single molecules of RNA polymerase. *Science* *282*, 902–907.

Wilson, K.A., Kalkum, M., Ottesen, J., Yuzenkova, J., Chait, B.T., Landick, R., Muir, T., Severinov, K., and Darst, S.A. (2003). Structure of microcin J25, a peptide inhibitor of bacterial RNA polymerase, is a lassoed tail. *J. Am. Chem. Soc.* *125*, 12475–12483.

Yin, H., Wang, M.D., Svoboda, K., Landick, R., Block, S.M., and Gelles, J. (1995). Transcription against an applied force. *Science* *270*, 1653–1657.

Yuzenkova, J., Delgado, M., Nechaev, S., Savalia, D., Epshtein, V., Artsimovitch, I., Mooney, R.A., Landick, R., Farias, R.N., Salomon, R., et al. (2002). Mutations of bacterial RNA polymerase leading to resistance to microcin j25. *J. Biol. Chem.* *277*, 50867–50875.

Zhang, G., Campbell, E.A., Minakhin, L., Richter, C., Severinov, K., and Darst, S.A. (1999). Crystal structure of *Thermus aquaticus* core RNA polymerase at 3.3 Å resolution. *Cell* *98*, 811–824.